Successive magnetic ordering of the Tb sublattices in $Tb_3Pd_{20}Si_6$

1999 J. Phys.: Condens. Matter 11 2929

(http://iopscience.iop.org/0953-8984/11/14/009)

J. Phys.: Condens. Matter **11** (1999) 2929–2936. Printed in the UK PII: S0953-8984(99)01103-0

Successive magnetic ordering of the Tb sublattices in $Tb_3Pd_{20}Si_6$

T Herrmannsdörfer†‖, A Dönni‡, P Fischer†, L Keller†, G Böttger†¶, M Gutmann†, H Kitazawa§ and J Tang§

† Laboratory for Neutron Scattering, ETH Zürich and Paul Scherrer Institute, CH-5232 Villigen PSI, Switzerland

‡ Department of Physics, Niigata University, Niigata 950-2181, Japan

§ National Research Institute for Metals (NRIM), Tsukuba 305-0047, Ibaraki, Japan

Received 20 January 1999

Abstract. The chemical and magnetic structures of the intermetallic compound $Tb_3Pd_{20}Si_6$ were studied by means of bulk magnetic measurements and neutron diffraction. The crystal structure of $Tb_3Pd_{20}Si_6$ was confirmed to be isotypic with that of $Ce_3Pd_{20}Si_6$, space group $Fm\bar{3}m$, No 225, with Tb being located at the two crystallographic sites 4a and 8c. The compound undergoes two successive second-order magnetic phase transitions at the Néel temperatures $T_{N1} = 10.2$ K and $T_{N2} = 4.1$ K. Below T_{N1}, the 8c sites order in an antiferromagnetic sequence with a magnetic propagation vector $\boldsymbol{k}_1 = [1, 1, 1]$, leaving the 4a sites disordered down to T_{N2}, where additional antiferromagnetic ordering of the 4a sites sets in according to $\boldsymbol{k}_2 = [0, 0, 1]$.

1. Introduction

For the new class of the ternary intermetallic compounds $R_3Pd_{20}Si_6$ (R = all rare earths) and $R_3Pd_{20}Ge_6$ (R = light rare earths), exceptional electronic and magnetic phenomena like the heavy-fermion behaviour of $Ce_3Pd_{20}Si_6$, which can be classified as one of the heaviest Kondo compounds with $\gamma = 8$ J mol^{-1} K^{-2} per Ce atom at 0.2 K [1], and the quadrupolar ordering of Ce in $Ce_3Pd_{20}Ge_6$ below $T_Q \approx 1.2$ K [2] have been reported. The cubic crystal structure of these compounds with space group $Fm\bar{3}m$, No 225, $Z = 4$, is an ordered derivative of the $Cr_{23}C_6$-type structure [3] and the magnetic rare-earth atoms occupy the two crystallographic sites 4a and 8c, both with cubic site symmetry, but with different coordinations.

For the $R_3Pd_{20}Si_6$ compounds, systematic bulk magnetic and transport measurements [4] revealed that the rare-earth ions are in the trivalent state and that magnetic order usually occurs in the mK temperature range. The compounds with R = Nd, Sm, Gd, Tb, Dy, and Ho exhibit two magnetic phase transitions and the higher and lower ordering temperatures both follow the de Gennes scaling. The compounds with R = Ce, Pr, Er, Tm, and Yb show only one magnetic phase transition and deviate from the de Gennes scaling. For the $R_3Pd_{20}Ge_6$ compounds, the magnetic properties are found to be rather unusual. $Ce_3Pd_{20}Ge_6$ shows quadrupolar ordering [2], $Pr_3Pd_{20}Ge_6$ exhibits a non-magnetic crystalline-electric-field ground-state doublet Γ_3 and magnetic order at $T_N = 0.2$ K is induced by exchange interactions [5, 6], and $Nd_3Pd_{20}Ge_6$ is the only system with three successive magnetic phase transitions [7].

‖ Author to whom any correspondence should be addressed. E-mail address: thilo.herrmannsdoerfer@psi.ch.

¶ Present address: Laboratory for Crystallography, ETH Zürich, CH-8092 Zürich, Switzerland.

0953-8984/99/142929+08$19.50

In this work, we have chosen $Tb_3Pd_{20}Si_6$ as the best representative of the $R_3Pd_{20}X_6$ (X = Ge, Si) series for investigating in detail the magnetic ordering by powder neutron diffraction. Besides $Gd_3Pd_{20}Si_6$ ($T_{N1} = 18.2$ K, $T_{N2} = 3.6$ K), which is not suitable for neutron scattering experiments, $Tb_3Pd_{20}Si_6$ ($T_{N1} = 10.2$ K, $T_{N2} = 4.1$ K) has the highest ordering temperatures, which are accessible with a ^{4}He cryostat. In addition, due to the value $g\mu_B J = 9.0\ \mu_B$ for Tb^{3+}, we can expect a large ordered magnetic Tb moment leading to strong magnetic neutron Bragg intensities which allow an accurate determination of the magnetic structures.

2. Experimental procedure

A polycrystalline sample of $Tb_3Pd_{20}Si_6$ was prepared by arc melting stoichiometric amounts of the pure elements (Tb: 3N; Pd: 3N5; Si: 7N) in an argon atmosphere and subsequent annealing in an evacuated quartz tube for 120 hours at 800 °C. The annealed sample was examined by powder x-ray diffraction and found to be single phased. The temperature variation of the specific heat, $c_p(T)$, was measured between 1.5 K and 25 K by a semi-adiabatic heat pulse method. The dc magnetic susceptibility $\chi(T) \equiv M/H$ was investigated between 1.9 K and room temperature for an external magnetic field of 0.1 T, using a Quantum Design SQUID magnetometer.

For the neutron diffraction experiments, the sample was ground to a fine powder and enclosed under a helium atmosphere in a vanadium cylinder of 10 mm diameter. Neutron diffraction data were collected on the high-resolution powder diffractometer D1A at the Institute Laue–Langevin, Grenoble, France, and on the double-axis multi-counter diffractometer DMC at the Swiss Spallation Neutron Source SINQ, Villigen, Switzerland. The data were taken at various temperatures in the paramagnetic and in the magnetically ordered states using a standard ILL orange cryostat. On D1A, a wavelength of $\lambda = 2.483$ Å ($(\sin\Theta)/\lambda \leqslant 0.40$ Å^{-1}) was selected by the 004 reflection of a vertically focusing Ge monochromator. A pyrolytic graphite filter was placed between the monochromator and the sample in order to reduce higher-order contamination. On DMC, $\lambda = 2.560$ Å ($(\sin\Theta)/\lambda \leqslant 0.27$ Å^{-1}) from the 002 reflection of a focusing graphite monochromator with a pyrolytic graphite filter was used. Typical counting times were 10 h per temperature on D1A for examinations of the chemical and magnetic structures and 1 h per temperature on DMC for detailed studies of the temperature variation of the magnetic intensities.

Rietveld refinements of the diffraction data were carried out for the range 0.04 Å$^{-1} \leqslant (\sin\Theta)/\lambda \leqslant 0.40$ Å^{-1} with the program FullProf [8], using the internal scattering length and magnetic form factor tables. The data were corrected for absorption by applying the measured value of $\mu r = 0.33$ for $\lambda = 2.483$ Å to the built-in correction function. The background was modelled by a third-order polynomial and the intensity profiles by the Thompson–Cox–Hastings pseudo-Voigt function [9].

3. Results

3.1. Macroscopic transport and magnetic properties

The results of the specific heat and susceptibility measurements are shown in figure 1, together with integrated neutron intensities of selected magnetic reflections from the diffraction measurements made on DMC. The macroscopic measurements on our $Tb_3Pd_{20}Si_6$ sample are in good overall agreement with those reported in reference [4].

Two well defined peaks, corresponding to magnetic phase transitions at the Néel temperatures T_{N1} and T_{N2}, can be identified in the temperature variation of the specific heat.

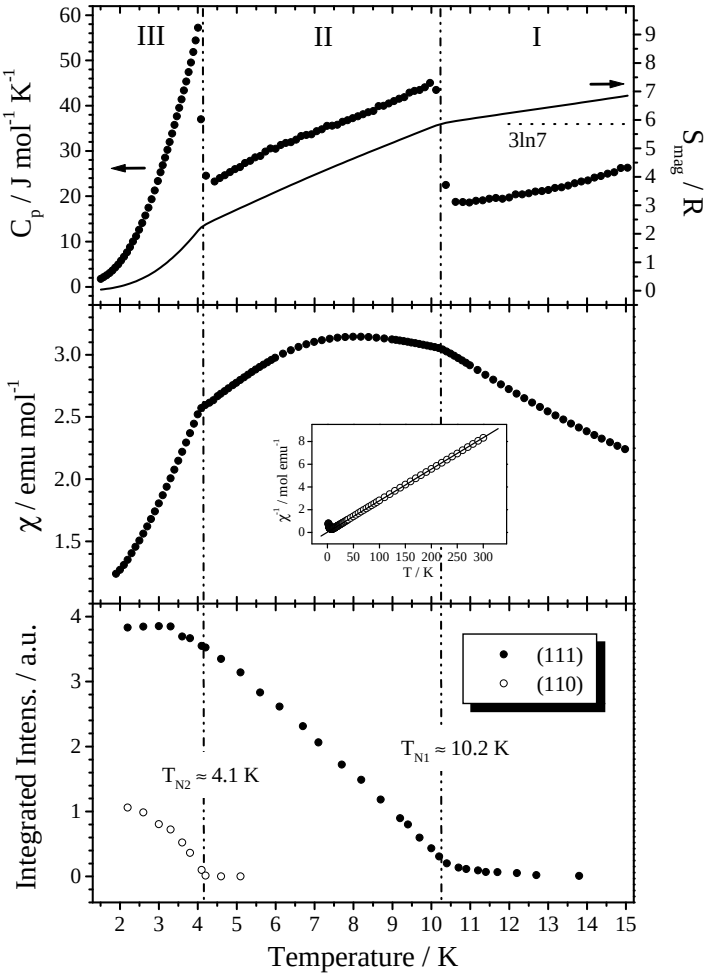

Figure 1. The temperature variation of the magnetic properties of $Tb_3Pd_{20}Si_6$. The two transition temperatures, defining the regions I to III, are indicated by dashed lines. Top: specific heat $c_p(T)$ (left-hand scale) and magnetic entropy $S_{mag}(T)/R$ (right-hand scale). Middle: magnetic susceptibility $\chi(T)$, with a linear Curie–Weiss fit shown in the inset. Bottom: integrated DMC neutron intensities of the magnetic (111) and (110) Bragg reflections, which are proportional to the squares of the magnetic moments on the 8c and 4a sites, respectively. The error bars of the integrated intensities are of the size of the data points and are therefore omitted.

They define three temperature regions, which will be denoted as I, II, and III in the following. Between T_{N1} and T_{N2}, no additional ordering is indicated from $c_p(T)$. This is in contrast to the situation found for $Nd_3Pd_{20}Ge_6$, which is the only member of the $R_3Pd_{20}X_6$ series with another magnetic phase between T_{N1} and T_{N2} [7]. Under the influence of the crystalline electric field (CEF) of the surrounding ions, the $(2J + 1)$-fold degeneracy of the rare-earth J-multiplets is partly lifted. For the cubic symmetry of the 4a and 8c sites (see table 1), the 13-fold-degenerate ground state of the Tb^{3+} ion, $^7F_6$, splits into two singlets Γ_1 and Γ_2, one doublet Γ_3, and three triplets Γ_4, $\Gamma_5^{(1)}$, and $\Gamma_5^{(2)}$. We calculated the magnetic entropy per formula unit by numerically integrating the experimental values of c_p/T (figure 1). The contribution to S_{mag}/R from temperatures lower than 1.5 K was estimated from the expression given in

Table 1. Refined structural parameters and selected interatomic distances of $Tb_3Pd_{20}Si_6$, space group $Fm\bar{3}m$, No 225, $Z = 4$, as obtained from D1A neutron powder diffraction data at $T = 14.6$ K. a: lattice parameter. R_{wp} and $R_{I,N}$: agreement indices concerning the weighted-profile and integrated neutron intensities, respectively. R_{exp}: value expected from the counting statistics. $\chi^2 = (R_{wp}/R_{exp})^2$: goodness of fit. x, y, z: fractional coordinates. B: isotropic temperature factor; the B of the Tb atoms were fixed at zero. Within error limits, the lattice parameter a was found to be constant over the temperature range between 14.6 K and 1.5 K.

T/K	a/Å	R_{wp}	$R_{I,N}$	R_{exp}	χ^2
14.6	12.154(5)	0.0441	0.0252	0.0302	2.13
Atom	Site symmetry	x	y	z	B/Å^2
Tb1 4a	$m\bar{3}m$	0	0	0	0
Tb2 8c	$\bar{4}3m$	1/4	1/4	1/4	0
Pd1 32f	. 3m	0.3840(1)	0.3840(1)	0.3840(1)	0.2(1)
Pd2 48h	m .m 2	0	0.1735(1)	0.1735(1)	0.2(1)
Si1 24e	4m .m	0.2678(2)	0	0	0.2(1)
Atoms	Distance/Å	No of bonds	Atoms	Distance/Å	No of bonds
Tb1–Tb1	8.594(4)	12	Tb2–Tb1	5.263(2)	4
Tb1–Tb2	5.263(2)	8	Tb2–Tb2	6.077(3)	6
Tb1–Pd2	2.977(3)	12	Tb2–Pd1	2.820(3)	4
Tb1–Si1	3.254(3)	6	Tb2–Pd2	3.313(1)	12

Table 2. Summary of the magnetic properties of $Tb_3Pd_{20}Si_6$ and $Nd_3Pd_{20}Ge_6$. μ_{eff}: effective magnetic moment; Θ_p: Curie temperature; T_N: Néel temperature; $\boldsymbol{k}$: magnetic propagation vector; μ: ordered magnetic moment; α: angle between $\boldsymbol{k}$ and $\boldsymbol{\mu}$. —: not determined. $*$: cannot be determined from a zero-field neutron powder diffraction experiment due to configurational symmetry [11]. Note that $Nd_3Pd_{20}Ge_6$ has a third magnetic phase transition at $T_N = 1.4$ K [7].

Reference:	$Tb_3Pd_{20}Si_6$ (this work)	$Tb_3Pd_{20}Si_6$ [4]	$Nd_3Pd_{20}Ge_6$ [6, 7]	$Nd_3Pd_{20}Ge_6$ [13]
μ_{eff}/μ_B, free ion	9.72	9.72	3.62	3.62
Curie–Weiss fit:				
μ_{eff}/μ_B	9.82(3)	9.59	—	3.60
Θ_p/K	−1.4(9)	2.69	—	—
Magnetic structure of 8c site:				
T_{N1}/K	10.2	10.2	1.75	1.7
$\boldsymbol{k}_1$	[1, 1, 1]	—	[1, 1, 1]	[1, 1, 1]
α_1	$*$	$*$	$*$	$*$
μ_1/μ_B	4.25(3) (8.7 K) 7.10(3) (5.4 K) 8.26(3) (1.5 K)	—	2.4 (0.3 K)	—
Magnetic structure of 4a site:				
T_{N2}/K	4.1	4	0.54	0.6
$\boldsymbol{k}_2$	[0, 0, 1]	—	[0, 0, 1]	[0, 0, 1]
α_2	0°	—	90°	—
μ_2/μ_B	8.42(4) (1.5 K)	—	2.2 (0.3 K)	—

reference [4], $c_{mag} = \alpha T^3 \exp(-\delta/T) + A/T^2$, with $\alpha = 1.45$ J mol^{-1} K^{-4}, $\delta = 1.38$ K, and $A = 0.59$ J K mol^{-1}, to be 0.042. At the upper transition temperature T_{N1}, the value of S_{mag}/R is very close to $3\ln(7)$. From this it follows that there are seven CEF levels below the energy of $k_B T_{N1} = 0.88$ meV. If we describe the CEF level scheme following Lea *et al* [10]

with the parameters W and x, and if we make the simplifying assumption that both Tb sites 4a and 8c have the same crystal-field splitting, we find that the lowest CEF levels are two triplets and one singlet, corresponding to an x-value >0.2 or <-0.55. This result is in contrast to an extrapolation of the crystal-field parameters from $Nd_3Pd_{20}Ge_6$ as published by Dönni *et al* [7] to $Tb_3Pd_{20}Si_6$, from which the lowest levels are expected to be the doublet Γ_3, followed by the triplet $\Gamma_5^{(1)}$, and the singlet Γ_2, with an energy splitting of as little as 0.9 meV. It is clear that neither our measurement of the magnetic entropy nor the extrapolation can give a conclusive answer as regards the CEF ground state present in $Tb_3Pd_{20}Si_6$. Moreover, the simplifying assumption that the crystal-field splitting is the same for both Tb sites is not expected to be justified. Further inelastic neutron scattering experiments are planned for the near future to reveal the actual CEF level scheme.

The magnetic susceptibility exhibits a Curie–Weiss behaviour over a wide temperature range. From a linear fit of $\chi(T)$ between 20 K and 300 K, we derived a value of $\mu_{eff} = 9.82\,\mu_B$ for the effective magnetic moment of the Tb ions and $\Theta_p = -1.4$ K for the Curie temperature, indicating a weak antiferromagnetic interaction (see table 2 and the inset of figure 1). Kitagawa *et al* [4] reported $\mu_{eff} = 9.59\,\mu_B$ and $\Theta_p = 2.69$ K, the latter suggesting a weak ferromagnetic ordering. Our value of μ_{eff} is slightly higher than the theoretical one for a free Tb^{3+} ion with the ground multiplet magnetic moment

$$\mu_{eff} = g\sqrt{J(J+1)}\,\mu_B = 9.72\,\mu_B$$

and it is clear that the rare-earth ions in $Tb_3Pd_{20}Si_6$ can be viewed as behaving almost like free ions in the paramagnetic state. It may be assumed that the weak exchange interactions between the Tb ions are a key ingredient for the magnetic ordering described in the next subsection.

3.2. The chemical and magnetic structures of $Tb_3Pd_{20}Si_6$

From our neutron diffraction experiments on D1A, the chemical structure of $Tb_3Pd_{20}Si_6$ was confirmed to be isotypic with that of $Ce_3Pd_{20}Si_6$, the latter being determined by Gribanov *et al* [3]. The space group is $Fm\bar{3}m$ (No 225), with four formula units per crystallographic unit cell. The Tb ions are located at the two crystallographically non-equivalent sites 4a and 8c, both having cubic point symmetry, with relatively high coordination numbers of 18 and 16, respectively. Refined structural parameters and selected interatomic distances at $T = 14.6$ K are summarized in table 1. Other structural features have also been nicely described by several authors [3, 4, 7].

Figure 2 shows the refined neutron powder diffraction patterns of $Tb_3Pd_{20}Si_6$ at three temperatures corresponding to the paramagnetic region I and the two magnetically ordered phases II and III. There is an excellent agreement between the observed and the calculated intensities. Comparing the three patterns, one can clearly recognize the occurrence of additional neutron intensity exclusively at reciprocal-lattice points in region II and additional peaks at positions not corresponding to nuclear Bragg reflections in region III.

Similarly to the situation for $Nd_3Pd_{20}Ge_6$ as reported by Dönni *et al* [7], the magnetic scattering in region II only occurs at positions of nuclear Bragg reflections with indices all odd and can be indexed with a propagation vector $\boldsymbol{k}_1 = [1, 1, 1]$. Together with the fact that Tb atoms at the 8c sites contribute *only* to nuclear peaks with all even indices, whereas the 4a sites form a fcc sublattice and contribute to *both* even and odd reflections, it can be concluded that the 4a sites are disordered in the temperature region II, and that the magnetic moments at the 8c sites are ordered according to an antiferromagnetic sequence of ferromagnetic (1, 1, 1) planes along the [1, 1, 1] direction (figure 3).

Below T_{N2}, additional magnetic intensity occurs at non-nuclear positions and another antiferromagnetic ordering is to be expected in this region. From a FullProf powder matching

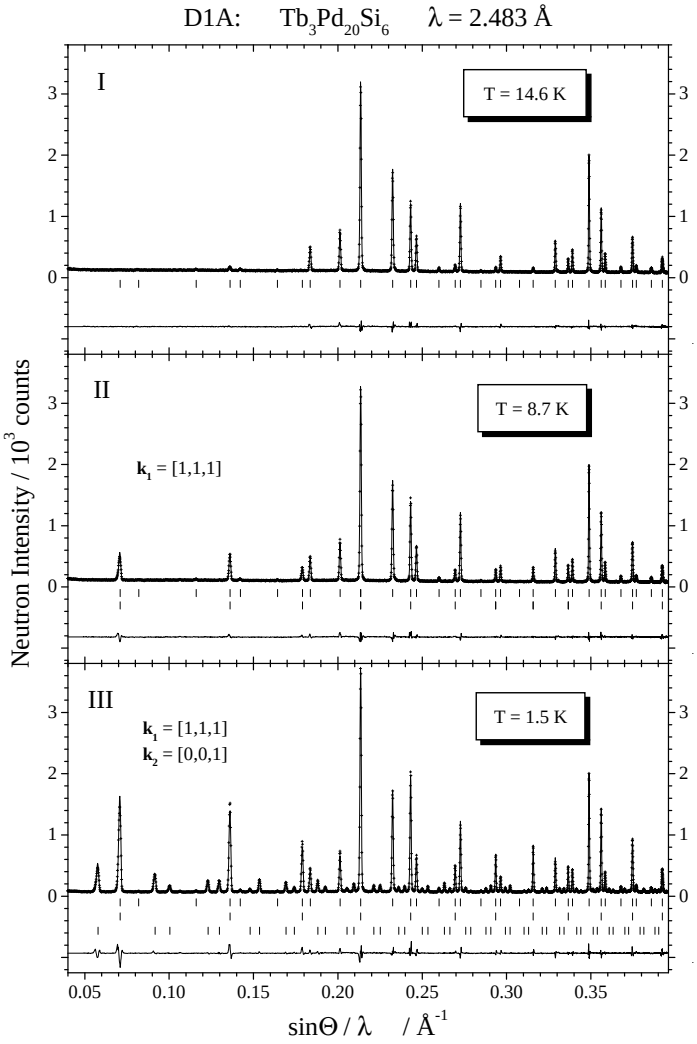

Figure 2. Observed, calculated, and difference neutron powder diffraction patterns of $Tb_3Pd_{20}Si_6$, obtained on D1A at three different temperatures. Top: the paramagnetic state (region I). Middle: the magnetically ordered state between T_{N1} and T_{N2} (region II). Bottom: the magnetically ordered state below T_{N2} (region III). The angular positions of Bragg reflections corresponding to the chemical and magnetic phases are indicated by markers. The refinements yielded χ^2-values of 2.1, 2.8, and 6.2, and weighted-profile R-values of 0.044, 0.051, and 0.075 for regions I, II, and III, respectively. Agreement values R_I concerning integrated nuclear and magnetic neutron intensities at $T = 1.5$ K, respectively: $R_{I,N} = 0.029$, $R_{I,M(\boldsymbol{k}_1)} = 0.032$, $R_{I,M(\boldsymbol{k}_2)} = 0.071$.

run it was seen that all magnetic peaks have indices with either $h, k, l = 2u, 2v, 2w + 1$ or $h, k, l = 2u+1, 2v+1, 2w$. Since the magnetic structure factor for the 4a sites, calculated with a propagation vector $\boldsymbol{k} = [0, 0, 1]$, has exactly the same reflection conditions, we conclude that below T_{N2} the 4a sites order antiferromagnetically according to $\boldsymbol{k}_2 = [0, 0, 1]$ in addition to the ordering of the atoms at the 8c sites. Basically, one could also apply a model with combinations of more than one propagation vector for each site. In our consideration, we shall restrict ourselves to the simplest model which is given above, since it leads to an excellent

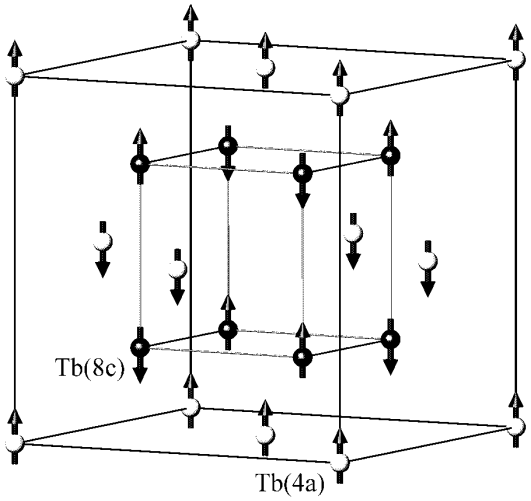

Figure 3. The magnetic structure of $Tb_3Pd_{20}Si_6$ below T_{N2}, showing the Tb atoms in the crystallographic unit cell at the Wyckoff positions 4a and 8c (white and dark circles, respectively). The antiferromagnetic ordering of the magnetic moments is indicated by arrows.

agreement with the experiment.

Given the propagation vectors $\boldsymbol{k}_1$ and $\boldsymbol{k}_2$, the configurational symmetry as defined by Shirane [11] is cubic for the 8c sites and tetragonal for the 4a sites. As a consequence, from our neutron powder experiment we cannot extract information about the orientation of the magnetic moments at the 8c sites with respect to the crystallographic axes. For the 4a sites, it is only possible to determine the angle between the direction of the magnetic moments and the c-axis. From our Rietveld refinement we found that the component of the magnetic moment at the 4a sites perpendicular to the c-axis is equal to zero within the parameter error, so the orientation of the magnetic moment is along the c-axis as illustrated in figure 3.

The bottom part of figure 1 shows the integrated neutron intensities of the magnetic (111) and (110) Bragg reflections corresponding to magnetic moments at the 8c and 4a sites, respectively, as measured on DMC at different temperatures. The distinct increase of magnetic intensity for the two reflections below T_{N1} and T_{N2} can be clearly seen. Due to local magnetic fluctuations, some magnetic intensity is already observed at around 12 K, which is approximately 2 K above the first ordering temperature $T_{N1} = 10.2$ K. The ordering at both rare-earth sites occurs in second-order magnetic phase transitions. At approximately 2 K, the magnetization is very close to saturation for both Tb sublattices. The refined values of the ordered Tb^{3+} magnetic moments from the D1A measurement at $T = 1.5$ K are $\mu = 8.26(3)\ \mu_B$ for the 8c sites and $\mu = 8.42(4)\ \mu_B$ for the 4a sites. Both values are close to the magnitude of the maximum possible ordered moment, $g\mu_B J = 9.0\ \mu_B$. It may be interesting to note that the ordering at the 4a sites sets in at a temperature at which the average magnetization at the 8c sites is already at a level of about 95% of saturation.

4. Summary and conclusions

We have studied the intermetallic rare-earth compound $Tb_3Pd_{20}Si_6$ by means of bulk magnetic measurements and neutron diffraction. Our results include the chemical structure and the magnetic structures of $Tb_3Pd_{20}Si_6$ down to 1.5 K, which represents the first complete magnetic structure determination of an $R_3Pd_{20}X_6$ (X = Ge, Si) compound. $Tb_3Pd_{20}Si_6$ is isotypic with $Ce_3Pd_{20}Si_6$ and crystallizes in the cubic space group $Fm\bar{3}m$, No 225, $Z = 4$. The Tb ions are located at the two crystallographic sites 4a and 8c, and show two successive magnetic phase

transitions at the Néel temperatures $T_{N1} = 10.2$ K and $T_{N2} = 4.1$ K. Below T_{N1}, the 8c sites order in an antiferromagnetic sequence with a propagation vector $\boldsymbol{k}_1 = [1, 1, 1]$, leaving the 4a sites disordered down to T_{N2}, where additional antiferromagnetic ordering of the 4a sites sets in according to $\boldsymbol{k}_2 = [0, 0, 1]$. Such successive ordering has been observed in only a few cases (see, for example, the case of Ho_3Ge_4 in reference [12]). To our knowledge, $Tb_3Pd_{20}Si_6$ is the first example where successive ordering at two different sites occupied by the same rare-earth element occurs with different propagation vectors. The values of the ordered magnetic moments at 1.5 K are 8.3 μ_B and 8.4 μ_B for the 8c and 4a sites, respectively. The orientation of the magnetic moments on the 8c site cannot be determined from neutron powder diffraction data since the configurational symmetry is cubic. For the tetragonal configurational symmetry of the 4a sites, the magnetic moments were found to be aligned along the *c*-axis.

The weak antiferromagnetic interaction as indicated by the specific heat and susceptibility measurements seems to be an important key to the understanding of the discrete ordering at the two rare-earth sites. As can be seen from table 1, the distance between the 8c sites, 6.08 Å, is much smaller than that between the 4a sites, 8.59 Å. This can explain why the ordering at the 8c sites set in at higher temperatures than that at the 4a sites. What remains uncertain is why the interaction between the 4a and 8c sites, which have a separation of 5.26 Å, does not lead to a coupling between the magnetic ordering at the two sites. One possible reason could be a cancellation of the magnetic nearest-neighbour interactions at the 4a site. This is in accordance with the observation that ordering at the 4a sites does not set in before the magnetization of the 8c sites is very close to saturation. Further inelastic neutron scattering experiments are planned in order to obtain information about the CEF level scheme of $Tb_3Pd_{20}Si_6$ from which the magnetic moment can be calculated and compared with the diffraction experiments. They may also serve as a basis for the extrapolation of crystal-field parameters to other members of the series in order to achieve a more comprehensive understanding of the observed phenomena.

Acknowledgments

We would like to thank A Furrer for stimulating discussions. Our work is partly supported by the Swiss National Science Foundation which is gratefully acknowledged

References

[1] Takeda N, Kitagawa J and Ishikawa M 1995 *J. Phys. Soc. Japan* **64** 387
[2] Kitagawa J, Takeda N and Ishikawa M 1996 *Phys. Rev.* B **53** 5101
[3] Gribanov A V, Seropegin Y D and Bodak O I 1994 *J. Alloys Compounds* **204** L9
[4] Kitagawa J, Takeda N and Ishikawa M 1997 *J. Alloys Compounds* **256** 48
[5] Keller L, Dönni A, Zolliker M and Komatsubara T 1999 *Physica* B at press
[6] Dönni A 1999 unpublished results
[7] Dönni A, Keller L, Fischer P, Aoki Y, Sato H, Fauth F, Zolliker M, Komatsubara T and Endoh Y 1998 *J. Phys.: Condens. Matter* **10** 7219
[8] Rodriguez-Carvajal J 1993 *Physica* B **192** 55
[9] Thompson P, Cox D E and Hastings J B 1987 *J. Appl. Crystallogr.* **20** 79
[10] Lea K R, Leask M J M and Wolf W P 1962 *J. Phys. Chem. Solids* **23** 1381
[11] Shirane G 1959 *Acta Crystallogr.* **12** 282
[12] Zaharko O, Schobinger-Papamantellos P, Ritter C, Janssen Y, Brück E, de Boer F R and Buschow K H J 1998 *J. Phys.: Condens. Matter* **10** 2881
[13] Kimura N, Tateiwa N, Nakayama M, Aoki H, Komatsubara T, Sakon T, Motokawa M, Koike Y and Metoki N 1999 *Physica* B at press